Pedosphere **36**(2): 655–668, 2026
doi: 10.1016/j.pedsph.2024.11.005
ISSN 1002-0160/CN 32-1315/P

Published by Elsevier B.V. and Science Press

PEDOSPHERE

www.elsevier.com/locate/pedosphere

Mechanistic understanding of biochar-induced inhibition of *Bacillus megaterium* growth and soil phosphorus solubilization

Yang LIU[1], Lihua ZHU[1], Junyuan ZHANG[1], Zhuo WEI[1,*], Xuhan HUANG[1], Christian E. W. STEINBERG[1,2], Hao QIU[3], Martina G. VIJVER[4], Jing ZHAO[1,*] and Willie J. G. M. PEIJNENBURG[4,5]

[1]*Yunnan Key Laboratory of Soil Carbon Sequestration and Pollution Control, Faculty of Environmental Science and Engineering, Kunming University of Science and Technology, Kunming 650500 (China)*
[2]*Institute of Biology, Freshwater & Stress Ecology, Humboldt University, Berlin 12437 (Germany)*
[3]*School of Environmental Science and Engineering, Shanghai Jiao Tong University, Shanghai 200240 (China)*
[4]*Institute of Environmental Sciences (CML), Leiden University, Leiden 2300RA (The Netherlands)*
[5]*National Institute of Public Health and the Environment (RIVM), Center for Safety of Substances and Products, Bilthoven 3720BA (The Netherlands)*

(Received August 25, 2024; revised October 11, 2024; accepted October 31, 2024)

ABSTRACT

Due to the complex composition of biochar and the potential interactions between its components, controversial results regarding its effects on soil phosphorus (P) solubilization have been reported. In this study, pinewood biochars were prepared at pyrolysis temperatures of 200 (BC200), 300 (BC300), 400 (BC400), 500 (BC500), and 600 (BC600) °C, and their dissolved (DBC200, DBC300, DBC400, DBC500, and DBC600, respectively) and particulate (WBC200, WBC300, WBC400, WBC500, and WBC600, respectively) fractions were prepared as well. An incubation experiment was conducted to investigate the effects of BCs, DBCs, and WBCs on the growth, acid (ACP) and alkaline (AKP) phosphatase activities, and metabolites and metabolic pathways of the P-solubilizing bacterium *Bacillus megaterium*. The results showed that the BCs, DBCs, and WBCs all negatively affected the growth and AKP activity of *B. megaterium*, and BC500, WBC500, BC400, and WBC400 had the greatest effects. Histidine metabolism was downregulated by BC400, and nucleotide metabolism was interfered by BC600. These negative effects of high-temperature biochars were caused by environmental persistent free radicals. In contrast, the effects of low-temperature biochars on cell proliferation and AKP activity were highly related to biochar metal contents. Using the independent action model, antagonistic effects were found between the biochar dissolved and particulate fractions in inhibiting *B. megaterium* growth, while these biochar fractions had synergistic effects on the inhibition of AKP activity. Overall, this study provides insights into how biochar adversely modulates microbial-mediated P solubilization.

Key Words: biochar fraction, cell proliferation, electron paramagnetic resonance, environmental persistent free radical, enzyme activity, non-targeted metabolic profiling, phosphorus-solubilizing bacteria

Citation: Liu Y, Zhu L H, Zhang J Y, Wei Z, Huang X H, Steinberg C E W, Qiu H, Vijver M G, Zhao J, Peijnenburg W J G M. 2026. Mechanistic understanding of biochar-induced inhibition of *Bacillus megaterium* growth and soil phosphorus solubilization . *Pedosphere*. **36**(2): 655–668.

INTRODUCTION

Phosphorus (P) is a macro element that is essential for the growth and development of plants, animals, and microorganisms. However, more than 90% of P in soil cannot be absorbed and utilized by soil organisms due to the high P-fixing capacity of most soils and the low solubilization of P (Alori *et al*., 2017; Ibáñez *et al*., 2021). Inorganic P is mainly present in soil as salts of calcium, aluminum, and iron (Fe), while organic P comes from decaying vegetation and microbial residues (Kour *et al*., 2021). The P-solubilizing bacteria (PSB) play an important role in decomposing or hydrolyzing insoluble P into bioavailable species. Particularly, PSB are capable of producing phosphatases, such as alkaline phosphomonoesterase, to catalyze the cleavage of the ester bond between the phosphate group and the organic moiety (*e.g*., inositol) in phosphomonoesters, thus inducing dephosphorylation and releasing orthophosphate (Khadem and Raiesi, 2017). This is a major regeneration pathway of bioavailable P in soil and aquatic ecosystems (Ammerman and Azam, 1985; Illmer and Schinner, 1992). By encoding the non-specific acid phosphatase (ACP) gene family and alkaline phosphatase (AKP) genes, *e.g*., *phoA*, *phoD*, and *phoX* (Cheng *et al*., 2023), PSB mediate ACP and AKP activities. In addition, PSB can secrete organic and inorganic acids (*e.g*., glycolic acid, malic acid, and carbonic acid) as secondary metabolites, which decrease soil pH and increase P release from insoluble inorganic forms such as calcium phosphate (Jakobsen *et al*., 2015; Kaur *et al*., 2016). Organic acids can be produced in three main metabolic pathways, *i.e*., glycolysis, the tricarboxylic acid cycle, and fatty acid metabolism, whilst the energy generated during the above

*Corresponding author. E-mail: weizhuo@kust.edu.cn, jzhao@kust.edu.cn.

metabolic processes can be used for adenosine triphosphate (ATP) synthesis (Mashek and Coleman, 2006; Sun *et al*., 2020). An alternative and less well-studied mechanism without organic acid production for mineral P solubilization is the release of protons by PSB accompanying respiration or ammonium assimilation (Illmer and Schinner, 1995). Thereupon, the activity of PSB seems to be very relevant to P utilization and biota growth in soil.

In recent years, biochar, a carbon (C)-rich material thermochemically converted from organic waste in the absence of oxygen (O), has been increasingly used in agricultural soils to improve soil fertility and crop production (Lehmann *et al*., 2006). However, existing studies have reported conflicting effects of biochar on soil microorganisms. On the one hand, some researchers believe that, by adding biochar prepared at high temperatures, microbes will gain more habitat or refuge from the increased soil porosity, specific surface area (SSA), and hydrophobicity (Quilliam *et al*., 2013a; Yuan *et al*., 2016). Alkaline ions in the dissolved substances of biochar can neutralize soil acidity (Shi *et al*., 2020), and some low-molecular-weight organic matters and P retained in low-temperature biochar can serve as a source of nutrients for microbes (Warnock *et al*., 2010; Hossain *et al*., 2020). On the other hand, low-temperature ($\leqslant$ 350 °C) biochar is prone to carry more organic pyrolytic byproducts that may be harmful such as short-C-chain aldehydes, furans, and ketones, while high-temperature biochar mainly carries aromatic compounds and long-chain hydrocarbons (Spokas *et al*., 2011). Moreover, metals, polycyclic aromatic hydrocarbons (PAHs), phenols, and environmental persistent free radicals (EPFRs) are well known toxic substances to most microbes and biomacromolecules, and their contents in the dissolved and particulate fractions of biochar are also closely related to the pyrolysis temperature (Quilliam *et al*., 2013b; Liu *et al*., 2018; Zhu *et al*., 2021). The above chemicals within biochar may pose high risks to microbial cells through both direct and indirect mechanisms. Directly, they can inactivate proteins and oxidize microbial membranes. Indirectly, they can induce the generation of reactive O species (ROS) (Li *et al*., 2022). Thereupon, the distribution of chemicals in the particulate and dissolved fractions of biochar may vary greatly across pyrolysis temperatures. This would lead to distinct antibacterial effects as well. Understanding the relationship between biochar physicochemical properties and the effects of its particulate and dissolved fractions would elucidate the mechanisms underlying the different biological effects of biochars prepared at different pyrolysis temperatures.

In addition, the biological effects of biochar would be much complicated due to the interactions between its particulate and dissolved fractions. For example, the EPFR content was found to be enhanced by dissolved organic matter (Pan *et al*., 2019). The independent action (IA) model based on "additivity" was used in the present study to assess the combined effects of biochar particulate and dissolved fractions on a P-solubilizing bacterium (Liu *et al*., 2021). The combined effects induced by mixture components, $E(c_{\mathrm{mix}})$, can be predicted by multiplying the responses of each component in the mixture without considering interactions using the IA model presented as Eq. 1:

$$E(c_{\mathrm{mix}}) = 1 - \prod_{i=1}^{n}(1 - E(c_i)) \quad (1)$$

where $E(c_i)$ is the effect of the ith component on the test organism. Statistically significant deviation of the observed combined effect from the value predicted using the IA model will be regarded as the potential interaction between the dissolved and particulate fractions of biochar.

Bacillus megaterium, a typical PSB widely present in all types of soils, was selected as the test organism in this study due to its strong ability in abundant enzyme production, spore forming, and P solubilization (Liang *et al*., 2020). To clarify the microbe-mediated P solubilizing process as influenced by biochar, a nested exposure experiment was designed to systematically investigate the effects of biochars produced at temperatures of 200 (BC200), 300 (BC300), 400 (BC400), 500 (BC500), and 600 (BC600) °C and their respective dissolved (DBC200, DBC300, DBC400, DBC500, and DBC600, respectively) and particulate (WBC200, WBC300, WBC400, WBC500, and WBC600, respectively) fractions on the growth, phosphatase activity, and cell metabolism of *B. megaterium*. Using the IA model (Eq. 1), the predicted effect of biochar was compared with the observed effect to test for an interaction between its dissolved and particulate fractions that is expected to significantly affect the overall effect of biochar. The primary objective of this study was to systematically explore the potential adverse effects of biochar on soil functional microorganisms, *e.g*., PSB. We hypothesized that i) the dissolved and particulate fractions of biochar may both have negative effects on PSB, ii) the extent of effect is dependent on the pyrolysis temperature, and iii) the extent of effect is intensified by the interaction between the dissolved and particulate fractions of biochar.

MATERIALS AND METHODS

Preparation and characterization of biochars and B. megaterium

The biochars, *i.e*., BC200, BC300, BC400, BC500, and BC600, used in the present study (BCs) were produced from pinewood (PW) pyrolyzed at 200, 300, 400, 500, and 600 °C, respectively, in a tube furnace (Tianjin Zhonghuan Electric Furnace Co., Ltd., China) under a dinitrogen atmosphere

for 2 h. After cooling to room temperature, all biochars as well as PW were ground, sieved to < 0.074 mm, and stored in brown glass bottles. To obtain the dissolved (DPWs, *i.e.*, DBC200, DBC300, DBC400, DBC500, and DBC600) and particulate (WPWs, *i.e.*, WBC200, WBC300, WBC400, WBC500, and WBC600) fractions, PW and BCs were each mixed with ultrapure water in vessels at mass ratios of 0.1%, 0.3%, and 0.5%, sealed, and placed on a shaker (25 °C, 150 r min^{-1}) for 7 d. After centrifugation (4 000 r min^{-1}, 30 min), the supernatants (*i.e.*, dissolved fractions) were passed through 0.45-μm filter membranes and stored at 4 °C for later use. The sediments (*i.e.*, particulate fractions) were washed with ultrapure water in a semi-continuous process until the solution pH was within 0.01 (Wongrod *et al.*, 2018) and oven-dried for later use.

The basic physicochemical properties of the BCs, WBCs, and DBCs were analyzed. pH was determined using a pH meter (Leici Instruments, China). The contents of nitrogen, hydrogen (H), O, C, and dissolved organic C (DOC) in PW and the BCs were measured using a Vario MICRO cube elemental analyzer (Elementar, Germany). The contents of manganese, copper (Cu), cadmium (Cd), chromium (Cr), zinc (Zn), nickel (Ni), arsenic (As), lead (Pb), and Fe in PW, DPW, the BCs, and the DBCs were determined using a NexION 350x inductively coupled plasma mass spectrometer (Perkin Elmer, USA). Phenolic compounds in PW, DPW, the BCs, and DBCs were determined using an 8890 gas chromatograph-mass spectrometer (GC-MS) (Agilent, USA). Phenolic compounds in PW, the BCs, DPW, and the DBCs were analyzed using a GC8890/5977B GC-MS (Agilent, USA), and PAHs in DPW and the DBCs were analyzed using an LC 2030 high-performance liquid chromatograph (Shimadzu, Japan).

Free radical signals were monitored on an A300-6/1 electron paramagnetic resonance (EPR) spectrometer (Bruker, Germany). To identify hydroxyl radicals (·OH) generated in biochar suspensions, 0.9 mL biochar suspension was mixed with 0.1 mL of 1.5 mol L^{-1} 5,5-dimethyl-1-pyrroline N-oxide (DMPO) solution and then analyzed by EPR (Fang *et al.*, 2014). The SSA of particles was determined using an ASAP2020 M surface area analyzer (Micromerities, USA). The surface morphology of particles was observed with a Gemini 300 scanning electron microscope (SEM) (ZEISS, Germany). The surface functional groups of PW, WPW, the BCs, and WBCs were analyzed using a Nicolet iS50 Fourier-transform infrared spectrometer (FTIR) (Thermo Fisher Scientific, USA).

To make sure that the P in biochar does not affect this experiment, the kinetics or thermodynamics of P leaching and adsorption of the BCs and WBCs were investigated. As shown in Fig. S1 (see Supplementary Material for Fig. S1), the total amounts of P leached from the BCs and the total amounts of P adsorbed by the BCs and WBCs were found to be very low.

The *B. megaterium* strain 1.10466 was purchased from China General Microbiological Culture Collection Center (Beijing) and inoculated in sterilized plates with pH 7 Luria-Bertani medium at 30 °C (Yu *et al.*, 2019). To determine the growth cycle of *B. megaterium* under P-deficient conditions, the bacteria were transferred to Pikovskaya's (PVK) medium (Pikovskaya, 1948) and placed on a rotary shaker (30 °C, 200 r min^{-1}) for 56 h. The PVK medium was composed of $Ca_3(PO_4)_2$ (5 g), $C_6H_{12}O_6$ (10 g), $(NH_4)_2SO_4$ (0.5 g), NaCl (0.3 g), $MgSO_4$ (0.3 g), KCl (0.3 g), $FeSO_4{\cdot}7H_2O$ (0.036 g), and $MnSO_4{\cdot}H_2O$ (0.03 g) dissolved in 1 L ultrapure water. The pH of the solution was adjusted to around 7 with HCl (5 mol L^{-1}). The bacterial density was measured three times every 4 h using a UV-2600 spectrophotometer (Shimadzu, Japan) at 600 nm, and the results were expressed as optical density at 600 nm (OD_{600}). As shown in Fig. S2 (see Supplementary Material for Fig. S2), the final OD_{600} was around 0.97, and the logarithmic phase of *B. megaterium* was from 4 to 20 h. The pre-culture time for the bacterium was thus set as 18 h. The shapes of the bacterial cells before and after their exposure to the BCs, DBCs, and WBCs were examined by SEM.

Experimental design

To determine the duration of exposure, *B. megaterium* was inoculated into a 100-mL flask containing 30 mL PVK medium and precultured on a shaker (30 °C, 200 r min^{-1}) for 18 h. Then, 1 mL of the above prepared bacterial seed liquid was inoculated into 30 mL sterilized PVK medium with 150 mg BC400 and kept on a shaker (30 °C, 200 r min^{-1}) for 7 d. The pH value, cell proliferation, and phosphatase activity of the suspension were measured every day. The exposure duration was determined to be 24 h, given the stable solution pH and the optimal bacterial growth and AKP activity (Figs. S3 and S4, see Supplementary Material for Figs. S3 and S4).

To investigate the effects of the BCs, DBCs, and WBCs on *B. megaterium*, a nested exposure experiment was conducted with different series of BCs, DBCs, and WBCs: i) BCs (BC200, BC300, BC400, BC500, and BC600) each at 4 doses (0% (control), 0.1%, 0.3%, and 0.5%) in PVK medium; ii) DBCs (DBC200, DBC300, DBC400, DBC500, and DBC600) prepared as the dissolved fractions of the above BC suspensions; and iii) WBCs (WBC200, WBC300, WBC400, WBC500, and WBC600) prepared as the particulate fractions of the above BC suspensions resuspended in the same volume of PVK medium. These different series of BCs, DBCs, and WBCs were sterilized (121 °C, 20 min) and cooled to room temperature. Then, bacterial seed liquid was inoculated and incubated on a shaker (30 °C, 200 r

min^{-1}) for 24 h to determine cell growth and conduct further metabolic analysis. All treatments were repeated three times. When divided by the average density of most mineral soils, *i.e.*, 2.6 g cm^{-3} (Yan *et al.*, 2018), the BC doses of 0.1%, 0.3%, and 0.5% can be roughly converted to soil amendment levels of 0.04%, 0.12%, and 0.20%, respectively.

Determination of cell proliferation and phosphatase activity inhibition

The cell counting kit-8 (CCK-8) (Beyotime Institute of Biotechnology, China) was used to determine cell proliferation under the influence of BCs, DBCs, and WBCs. According to the reaction principle of CCK-8 (Yang *et al.*, 2021), dehydrogenase transforms the CCK-8 reagent to orange formazan. To reduce potential interference from biochar, 5 mL cell suspension from each treatment was centrifuged (15 984 $\times$ g, 10 min) after incubation for 24 h, and 100 μL supernatant was added to 96-well plates, followed by 10 μL CCK-8 reagent. The plates were incubated at 30 °C for 4 h to ensure a thorough reaction. The optical density at 450 nm (OD_{450}) was measured using a WD-2102B automatic microplate spectrophotometer (Liuyi Biotechnology Co., Ltd., China) to represent the activity of dehydrogenase released into the supernatant after cell rupture or death. For adsorption correction, adsorption assays were performed to determine the adsorbed amount of dehydrogenase (30 U mg^{-1}, Aladdin, China) on BCs and WBCs. Thereupon, the higher the OD_{450} value or dehydrogenase activity, the more severe the cell decay or breakage due to BCs, DBCs, and WBCs. The inhibition rate of bacterial cell proliferation (IR_c) by BCs, DBCs, and WBCs was calculated as follows:

$$IR_c = \frac{OD_{450\_T} - OD_{450\_CK}}{OD_{450\_CK}} \times 100\% \quad (2)$$

where OD_{450_T} is the OD_{450} value of the BC, DBC, and WBC treatment (*i.e.*, 0.1%, 0.3%, or 0.5% dose), and OD_{450_CK} is the OD_{450} value of the no BC, DBC, or WBC addition treatment (*i.e.*, 0% dose).

For determination of phosphatase activity, 5 mL cell suspension from each treatment was centrifuged (15 984 $\times$ g, 10 min). The activities of ACP and AKP in the supernatant were respectively determined using the P0326 ACP assay kit and the P0321 M AKP assay kit (Beyotime Institute of Biotechnology, China). The optical density at 405 nm (OD_{405}) of the resulting solution was measured using a WD-2102B automatic microplate spectrophotometer (Liuyi Biotechnology Co., Ltd., China), and the generated amount of p-nitrophenol was determined according to the standard curve in Fig. S5 (see Supplementary Material for Fig. S5). The activity of ACP or AKP was expressed as the amount of generated p-nitrophenol. The higher the amount of generated p-nitrophenol, the higher the activity of phosphatase in the solution. The inhibition rate of ACP or AKP activity (IR_p) by BCs, DBCs, and WBCs was calculated as follows:

$$IR_p = \frac{PA_{CK} - PA_T}{PA_{CK}} \times 100\% \quad (3)$$

where PA_{CK} is the ACP or AKP activity in the no BC, DBC, or WBC addition treatment (*i.e.*, 0% dose), and PA_T is the ACP or AKP activity in the BC, DBC, or WBC addition treatment (*i.e.*, 0.1%, 0.3%, or 0.5% dose).

Non-targeted metabolic profiling

The non-targeted metabonomic analysis was performed to detect the differences in bacterial metabolites and P solubilization mechanism as influenced by biochar. Cell suspension treated with 0% and 0.5% BC200, BC400, and BC600 was centrifuged (999 $\times$ g, 10 min, 4 °C), and the supernatant was filtered through a 0.22-μm membrane, collected, and stored at −80 °C for liquid chromatography-mass spectrometry analysis. Quality control samples were prepared by taking 20 μL from each sample (An *et al.*, 2021). The sample preparation and subsequent metabolomic analysis were performed by the Personal Biotechnology Company (Shanghai, China) using a 1290 Infinity ultrahigh-pressure liquid chromatograph (Agilent, USA) coupled to a Triple TOF 6600 mass spectrometer (SCIEX, USA). Both positive and negative ion modes of electrospray ionization were used for detection. The XCMS package in the R 3.6.3 software (Lucent Technologies, USA) was used in peak identification, filtration, and alignment of raw data to obtain the data matrix. Orthogonal partial least-squares discriminant analysis model further served to obtain a value of the variable importance in the projection (VIP). The differentially expressed metabolites (DEMs) were selected with VIP > 1 and $P < 0.05$ in Student's t-test on the normalized peak areas. The Kyoto Encyclopedia of Genes and Genomes (http://www.kegg.jp/) was utilized to perform metabolic pathway analysis of identified metabolites.

Statistical analysis

Data were processed using the R 3.6.3 software (Lucent Technologies, USA) and analyzed using one-way analysis of variance at the probability level of $P < 0.05$. Means were separated using Fisher's least significant difference. Pearson correlation coefficients (r) were calculated to determine the relationships between the effects of BCs, WBCs, and DBCs and their chemical properties. The Origin 8.0 software (Origin Lab, USA) was used for figure plotting.

RESULTS AND DISCUSSION

Properties of biochars and biochar fractions

Both the chemical and structural compositions of the BCs, WBCs, and DBCs showed significant differences due

to different pyrolysis temperatures (Figs. S6 and S7, Tables SI–SV, see Supplementary Material for Figs. S6 and S7 and Tables SI–SV). As pyrolysis temperature increased, the pH, ash and C contents, and SSA of the biochar increased, while the DOC, O, and H contents decreased (Table SI), indicating the decomposition of organic compounds during pyrolysis. This result suggested a higher degree of charring, aromaticity, and stability of the biochar produced at a higher temperature, which was consistent with the general reported findings (Demirbas, 2004; Chen *et al*., 2012). However, no significant difference was observed in the FTIR spectra between PW and BC200 or between the BCs and WBCs (Fig. S6). Pyrolysis temperature affected the properties of the biochar. In particular, the signal intensity of biochar pyrolyzed at 400 °C showed an increase at 1 612–1 615 cm^{-1} (aromatic C=C stretching and C=O stretching of conjugated ketones and quinones) as compared to 300 °C (Uchimiya *et al*., 2011), while the signal intensity decreased at 1 730–1 734 cm^{-1} (–COOH stretching vibrations), 876 cm^{-1} (C–H stretching of aromatic compounds) (Yakout, 2017), 1 037–1 162 cm^{-1} (C–O stretching of aliphatics and C–H stretching of biopolymers) (Rafiq *et al*., 2016), and 1 030–1 160 cm^{-1} (C–O–C stretching of oxygenated functional groups of cellulose). These findings were caused by the rapid loss of O and H and the likely formation of an aromatic C-ring skeleton at about 400 °C, which could be confirmed by the coarser and more porous surface of BC400 as compared with PW (Fig. 1). These findings were also consistent with the results of elemental analysis (Table SI).

Effects of biochars and biochar fractions on the growth of B. megaterium

The effects of different doses of BCs, DBCs, and WBCs on the growth or proliferation of *B. megaterium* cells were examined based on dehydrogenase activity. The OD_{450} value (as an indicator of extracellular dehydrogenase activity) was reduced by 0.1% BC200, BC300, BC400, WBC200, and WBC300 (Fig. 2). This indicated a positive effect or hormesis of a low dose of biochar on the growth or proliferation of *B. megaterium*. In contrast, at a dose of 0.5%, BC500 had the strongest inhibitory effect on the bacterium, followed by BC300 and BC600. Similarly, the negative effects of 0.5% WBCs were in the sequence: WBC500 > WBC600 > WBC400 > WBC300 > WBC200. The influences of BCs and WBCs on OD_{450} were significantly positively correlated with biochar dose. However, although the DBCs also had significant adverse effects on *B. megaterium* growth, the effects were not dose-dependent. This suggested that certain components of the biochars may act as exohormones influencing *B. megaterium* growth, and these components were not primarily present in the dissolved fraction. The above results indicated that both the particulate and dissolved fractions of the biochars had negative effects on the growth of *B. megaterium*, with the former exhibiting a stronger effect.

Based on the results of the above exposure experiment, we selected the treatments of different fractions of biochar with the strongest inhibitory effect for morphology observation. The SEM images showed that the originally smooth and intact cell surface of *B. megaterium* (Fig. 3a) turned to be irregular, slender, wrinkled or even torn open after exposure to BC400 (Fig. 3c) and BC500 (Fig. 3e). The exposure to DBC400 caused cracks on cell membranes (Fig. 3j). This may be due to a higher extracellular salt concentration (Wang *et al*., 2017). In addition, the occurrence of cell aggregation was observed in the treatments of WBC400 (Fig. 3f) and WBC500 (Fig. 3g). Aggregation of bacterial cells usually occurs to defend against toxic substances in the environment (Anuj *et al*., 2020). The observation of cell aggregation suggested that the bacterial cells on the surfaces of WBC400 or WBC500 tried to avoid harmful substances distributed unevenly on WBC. Compared with BC400 (Fig. 3b), the number of cells at the division stage was higher in the BC500 treatment (Fig. 3d), indicating a slower growth rate. Overall, the above results indicated the toxicity to *B. megaterium* in the sequence: DBC400 < WBC400 ≈ WBC500 < BC400 ≈ BC500.

Effects of biochars and biochar fractions on phosphatase activity

The BCs, WBCs, and DBCs had significantly adverse

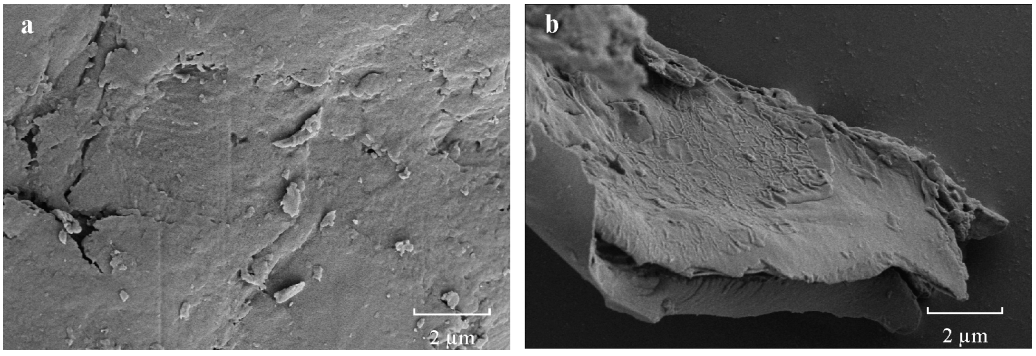

Fig. 1 Scanning electron microscopy images of pinewood (a) and biochar prepared from the pinewood pyrolyzed at 400 °C (b).

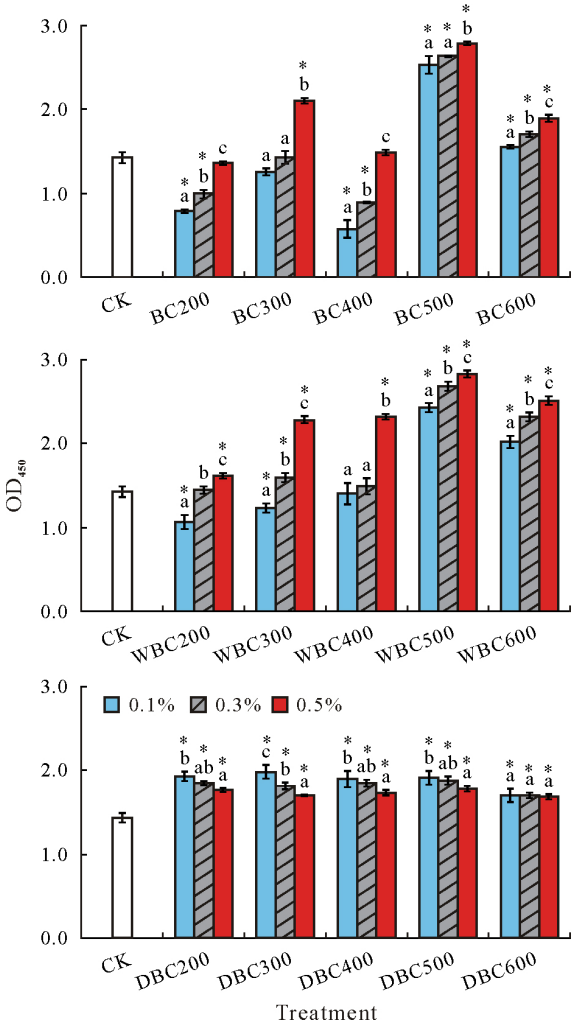

Fig. 2 Dehydrogenase activities, as indicated by the optical density at 450 nm (OD_{450}) of the cell counting kit-8 reaction solutions, of the P-solubilizing bacterium *Bacillus megaterium* in different treatments after 24-h incubation in Pikovskaya's medium with addition of 0% (control, CK), 0.1%, 0.3%, and 0.5% biochar (BC) prepared from pinewood pyrolyzed at 200 (BC200), 300 (BC300), 400 (BC400), 500 (BC500), and 600 (BC600) °C and their particulate (WBC200, WBC300, WBC400, WBC500, and WBC600, respectively) and dissolved (DBC200, DBC300, DBC400, DBC500, and DBC600, respectively) fractions. Error bars are standard errors of the means ($n = 3$). Different letters above the columns indicate significant differences between doses for the same BC or BC fraction at $P < 0.05$. An asterisk * indicates a significant difference between the treatment and CK at $P < 0.05$.

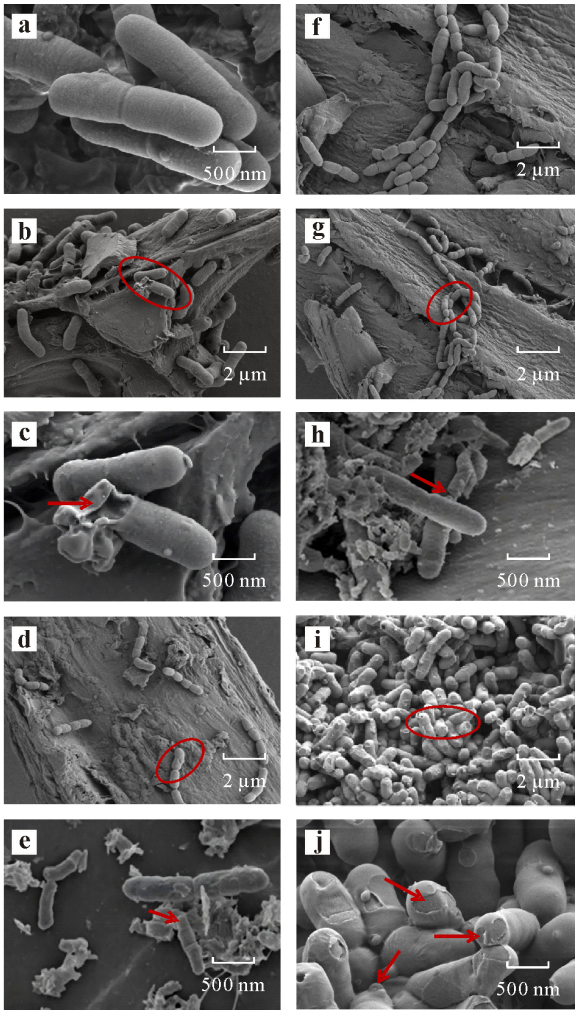

Fig. 3 Scanning electron microscopy images of the P-solubilizing bacterium *Bacillus Megaterium* after 24-h incubation in Pikovskaya's medium without (a) and with addition of 0.3% biochar prepared from pinewood pyrolyzed at 400 (BC400) (b and c) and 500 (BC500) (d and e) °C, the particulate fractions of 0.3% BC400 (f) and BC500 (g and h), and the dissolved faction of 0.3% BC400 (i and j). The arrows and circles indicate where the bacterial cells may be deformed or damaged.

effects on AKP activity (Fig. 4), which partially confirmed our hypothesis. The inhibitory effects of the BCs and WBCs increased with their increasing doses, but the inhibitory effects of the DBCs did not. The inhibitory effects of the BCs and WBCs on AKP activity were significantly stronger than those of the DBCs. This agreed well with the result of dehydrogenase activity (Fig. 2). Additionally, significant negative correlations (r value as low as -0.93) were found between the metal contents and AKP activity of BCs (Table SVI, see Supplementary Material for Table SVI). It is known that As^{3+}, Cd^{2+}, and Cr^{6+} trigger protein aggregation by directly interfering with protein folding and increasing mRNA mistranslation (Ozturk *et al.*, 2021). As demonstrated with *Escherichia coli*, a classical model bacterium, AKP is secreted in a monomeric form into the periplasmic space of the bacterium, where it dimerizes and becomes catalytically active (Bradshaw *et al.*, 1981). Metals in biochar may interfere with the dimerization process and prevent the formation of a catalytically active complex. However, this strong correlation was not found in the DBC or WBC treatments. Thus, we speculate that the strong contribution from metals in the BC treatments may be the result of the synergistic interaction between the particulate and dissolved fractions of biochar.

Relationships between the properties and effects of biochars and biochar fractions

The compositions/properties (*e.g.*, SSA and contents of

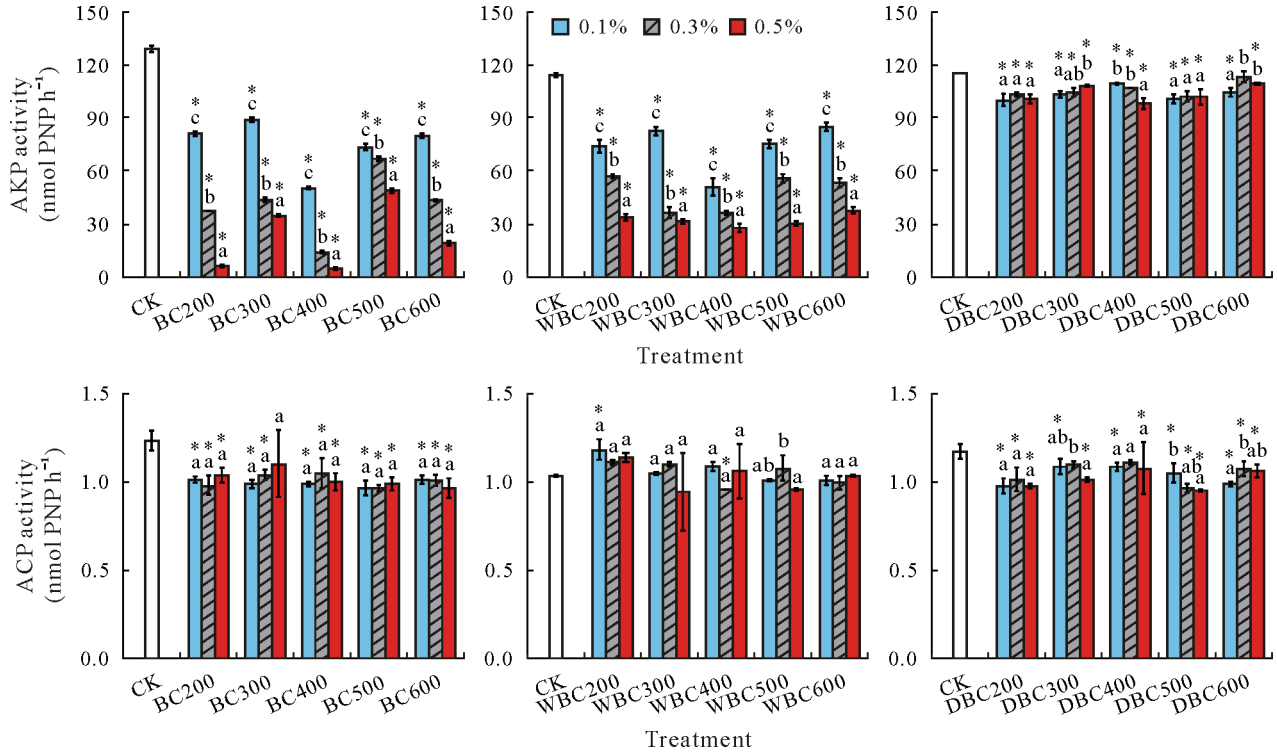

Fig. 4 Activities of alkaline (AKP) and acid (ACP) phosphatases of the P-solubilizing bacterium *Bacillus megaterium* in the 5-mL supernatants from different treatments after 24-h incubation in Pikovskaya's medium with addition of 0% (control, CK), 0.1%, 0.3%, and 0.5% biochar (BC) prepared from pinewood pyrolyzed at 200 (BC200), 300 (BC300), 400 (BC400), 500 (BC500), and 600 (BC600) °C and their particulate (WBC200, WBC300, WBC400, WBC500, and WBC600, respectively) and dissolved (DBC200, DBC300, DBC400, DBC500, and DBC600, respectively) fractions. Error bars are standard errors of the means ($n = 3$). Different letters above the columns indicate significant differences between doses for the same BC or BC fraction at $P < 0.05$. An asterisk * indicates significant difference between the treatment and CK at $P < 0.05$. PNP = *p*-nitrophenol.

EPFR, metals, and PAHs) of the BCs, WBCs, and DBCs and their correlations with dehydrogenase activity (OD_{450}) were analyzed to further determine the inhibitory mechanism on PSB. Significant DMPO-OH signals were observed for the BC400, BC500, BC600, WBC500, and WBC600 treatments, with BC500 and WBC500 having the highest intensities of ·OH (Fig. S8, see Supplementary Material for Fig. S8) and EPR signals (Fig. S7). Meanwhile, significant positive correlations between dehydrogenase activity (OD_{450} value) and EPR intensity ($r = 0.94$) and SSA ($r = 0.95$) were found for BC400, BC500, and BC600 (Table SVI). Similar correlations were also found for WBC400, WBC500, and WBC600 ($r = 0.76$ and 0.79, respectively). These results indicated that the toxic effects of high-temperature BCs and WBCs on PSB growth were most probably connected with the free radicals generated on the biochar particles and their SSAs. Similar results have also been reported by Lieke *et al*. (2018). These authors showed that low doses of EPFRs can trigger neurotoxicity in *Caenorhabditis elegans* even when the potentially toxic chemicals are not present in high enough concentrations. High-temperature pyrolysis causes asymmetric contraction of biochar and leads to the intensification of its aromatic structure, as well as the transition from a C-centered to an O- or C/O-centered free radical (Das *et al*., 2021). On the other hand, other characteristics of high-temperature biochar could also contribute to its high toxicity to PSB. For example, the low content of O-containing functional groups in high-temperature biochar can lead to a decrease in the repulsive force of biochar towards microorganisms (Suliman *et al*., 2017). A larger SSA of the high-temperature biochar may provide more opportunities for PSB cells to contact the free radicals with a high EPR intensity on the biochar surface (Fig. S7), resulting in oxidative damage to cell membranes (Zhang *et al*., 2022). For the low-temperature (200 and 300 °C) biochars, the contents of metals (Cu, Cd, Cr, Ni, and Zn) in the particulate and dissolved fractions of biochar, and the contents of PAHs in the dissolved fraction of biochar showed high positive correlations ($r \geqslant 0.69$) with *B. megaterium* dehydrogenase activity (OD_{450} value). Zhang *et al*. (2019) also reported that the toxicity of the dissolved fraction of low-temperature rice straw biochar was much higher than that of its high-temperature counterpart because of the presence of more toxic molecules such as PAHs. These toxic substances are stored in biochar without the possibility of volatilization, whilst they are soluble at low temperatures (Spokas *et al*., 2011). Therefore, the toxicity of the dissolved fraction is stronger than that of the particulate fraction. Clearly, apart from pyrolysis temperature, the feedstock of biochar could

also have a great influence on the toxicity to PSB. Moreover, our results also presented a significant ($P < 0.05$) positive correlation between biochar EPR intensity content and its toxicity to *B. megaterium* (Table SVI).

Although 0.1% BC200, BC300, and BC400 promoted the proliferation of *B. megaterium* cells (Fig. 2), they inhibited ACP and AKP activities (Fig. 4), with BC400 having the strongest inhibitory effect. Only 51% of the inhibited AKP activity can be explained by the decreased proliferation of *B. megaterium* cells (Fig. S9, see Supplementary Material for Fig. S9). The above difference in inhibition between cell proliferation and P solubilization may be because dehydrogenase is an intracellular enzyme protected by the cell membrane barrier (Anthony, 1992), while phosphatase is an extracellular enzyme more susceptible to interference from external substances (Park *et al*., 2022). In addition, the adverse effect of biochar particles was dose-dependent for AKP but not for ACP. This may be because the activity of AKP in CK was more than 100 times that of ACP in the first 24 h. Consequently, minor secretion of ACP would be noticeable. The activity of ACP showed an increasing trend only when cultured until the 6th day (Fig. S4), although the solution pH remained slightly acidic during this period (Fig. S3d). Thus, the secretion of ACP was supposed to be stimulated at a later stage of PSB growth and reproduction with more extracellular P-containing organic matter in the system. These results indicated that the main mechanism of P solubilization by *B. megaterium* is the secretion of AKP or organic acids rather than ACP in the presence of PW biochar.

Adverse effects from biochar particulate and dissolved fractions

The measured inhibition rates of *B. megaterium* cell proliferation and AKP activity were compared with their predicted values using the IA model based on additivity. Most of the measured inhibition rates were either significantly lower or higher than their predicted values (Table I). These significant deviations from additivity may very likely be due to interactions between the particulate and dissolved fractions of the biochars. Notably, the inhibition rates of cell proliferation in the WBC treatments were much higher than those in the BC treatments, especially for the 0.3% and 0.5% doses (Fig. 5). Meanwhile, the corresponding DBC treatments all showed inhibitory effects on cell proliferation. These results demonstrated that the dissolved fractions of BC200, BC300, BC400, and BC600 significantly reduced the inhibitory effects of their particulate fractions on cell proliferation. In other words, antagonistic interactions occurred between the dissolved and particulate fractions of the BCs on influencing PSB growth. Zhang *et al*. (2022) explained that humic acid can alleviate the toxicity of pine needle biochar to *Scenedesmus obliquus* by reducing the aggregation and adsorption of biochar on cell surfaces. In addition, the proliferation of *B. megaterium* cells can be stimulated by biochar at low doses, *e.g*., 0.1% BC200, BC300, and BC400 and 0.3% BC200 and BC400, in a relatively simple aqueous solution system. This is the so-called hormesis or stimulation effect (Zhu *et al*., 2019), which occurs for most chemicals and has been considered as a commonality across dose-response relationships (Calabrese and Baldwin, 2003). In complex soil environments, due to the strong adsorption of soil particles (Ling *et al*., 2002), the contact opportunity between bacterial cells and biochar particles or their dissolved substances will be lower as compared to solutions. The threshold dose of biochar application and the duration for inducing unwanted effects are supposed to be raised as well. Further studies could thus focus on extrapolating our findings to longer-term exposures and soil cultivation experiments.

TABLE I

Measured and predicted inhibition rates of cell proliferation and alkaline phosphatase activity of the P-solubilizing bacterium *Bacillus megaterium* in different treatments after 24-h incubation in Pikovskaya's medium with addition of 0.1%, 0.3%, and 0.5% pinewood biochar pyrolyzed at 200 (BC200), 300 (BC300), 400 (BC400), 500 (BC500), and 600 (BC600) °C

Biochar	0.1%		0.3%		0.5%	
	Measured	Predicted	Measured	Predicted	Measured	Predicted
	%					
	Cell proliferation					
BC200	−45.53 ± 1.17[a] a[b]	19.43 ± 0.92b	−30.67 ± 0.55a	33.06 ± 0.99b	−4.66 ± 1.42a	37.67 ± 1.72b
BC300	−11.79 ± 3.54a	31.67 ± 1.04b	1.43 ± 0.55a	38.91 ± 1.07b	47.70 ± 2.08a	68.99 ± 2.62b
BC400	−60.02 ± 0.84a	34.16 ± 0.47b	−38.23 ± 2.00a	36.12 ± 0.36b	3.79 ± 0.84a	74.61 ± 2.53b
BC500	77.85 ± 1.94a	83.66 ± 0.93a	84.99 ± 1.98a	87.68 ± 0.81a	96.42 ± 2.57a	96.56 ± 3.71a
BC600	9.08 ± 2.16a	56.19 ± 1.01b	20.00 ± 2.82a	69.22 ± 3.52b	32.41 ± 0.87a	80.78 ± 2.72b
	Alkaline phosphatase activity					
BC200	37.57 ± 0.92a	44.76 ± 0.29b	71.18 ± 0.90b	55.25 ± 1.78a	95.57 ± 0.54b	74.25 ± 1.68a
BC300	36.07 ± 1.55b	31.92 ± 0.96a	71.51 ± 1.27b	68.17 ± 0.77a	75.68 ± 0.67b	71.44 ± 0.97a
BC400	60.66 ± 1.35a	58.53 ± 1.99a	88.66 ± 0.52b	70.08 ± 3.56a	96.01 ± 0.33b	78.53 ± 2.87a
BC500	42.85 ± 0.61a	42.94 ± 0.74a	57.26 ± 1.75b	47.89 ± 0.37a	76.28 ± 0.98b	63.52 ± 3.00a
BC600	38.86 ± 1.85b	31.44 ± 0.22a	66.52 ± 1.25b	53.56 ± 2.61a	85.26 ± 0.72b	69.56 ± 2.11a

[a] Mean ± standard error ($n = 3$).

[b] Different letters indicate significant differences between the measured and predicted values for a same BC and dose at $P < 0.05$.

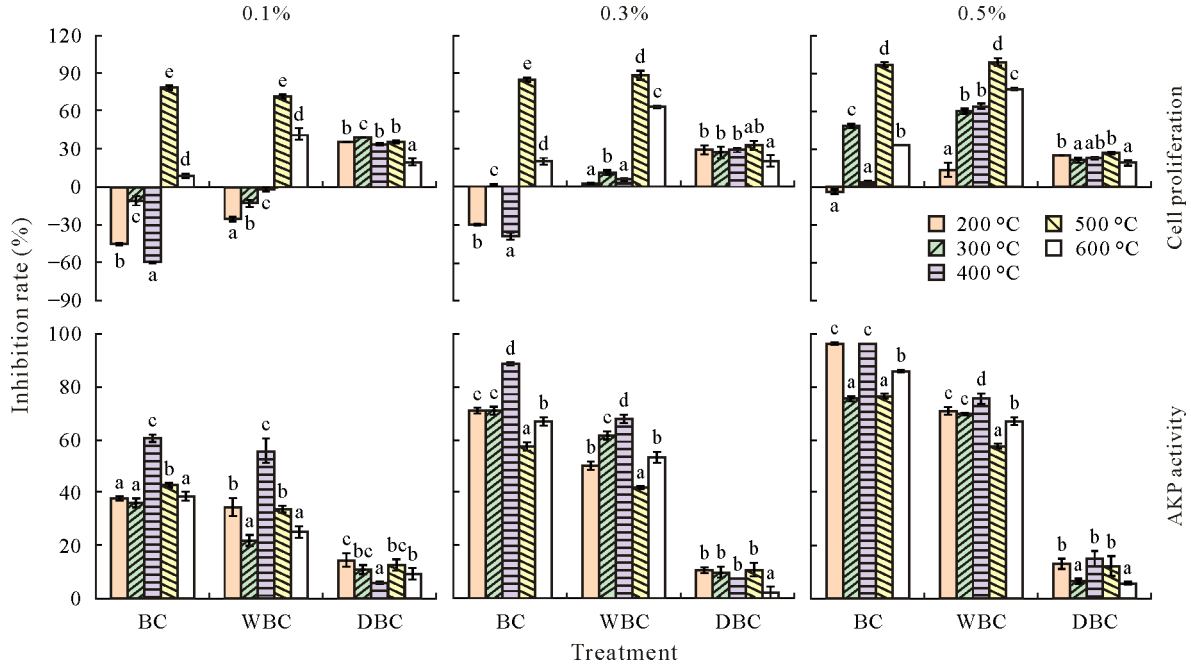

Fig. 5 Inhibition rates of cell proliferation and alkaline phosphatase (AKP) activity of the P-solubilizing bacterium *Bacillus megaterium* in different treatments after 24-h incubation in Pikovskaya's medium with addition of 0.1%, 0.3%, and 0.5% pinewood biochars (BCs) pyrolyzed at 200, 300, 400, 500, and 600 °C and their particulate (WBCs) and dissolved (DBCs) fractions. Error bars are standard errors of the means ($n = 3$). Different letters above the columns indicate significant differences between pyrolysis temperatures for the same BC or BC fraction at $P < 0.05$.

In contrast, for AKP activity, most of the measured inhibition rates of the BC treatments were significantly higher than the values predicted using the IA model, especially for the 0.3% and 0.5% doses (Table I). The corresponding inhibition rates of AKP activity in the WBC treatments were lower than those in the BC treatments. These findings indicated that the presence of dissolved substances of biochar significantly enhanced the WBC effects on *B. megaterium* AKP activity, especially at high doses. This may be caused by the synergistic interactions between the compounds attached to biochar particles and the dissolved substances released from biochar (Pan *et al*., 2019; Li *et al*., 2022). The findings also indicated that the content of a single substance in biochar is not enough to represent the safety of the entire biochar due to the common occurrence of interactions among biochar components. For example, although the contents of Cu, Cd, Cr, Ni, Zn, Pb, and As in the BCs (Table SII) met the threshold criteria for soil application (International Biochar Initiative, 2015), the inhibitory effects of the BCs on AKP activity could still be observed in a relatively simple aqueous solution system. This indicated that the potential risks of biochar may increase under waterlogging conditions.

Effects of biochars and biochar fractions on B. megaterium metabolism

Non-targeted metabolic profiling revealed a total of 139 (79 upregulated and 60 downregulated), 77 (24 upregulated and 53 downregulated), and 49 (14 upregulated and 35 downregulated) DEMs in the BC200, BC400, and BC600 treatments, respectively (Figs. S10 and S11, see Supplementary Material for Figs. S10 and S11). Interestingly, although the number of DEMs was the largest in the BC200 treatment, the proportion of downregulated ones in the total was the highest in the BC600 treatment (71%), followed by the BC400 treatment (69%) and the BC200 treatment (43%). This result was consistent with the observations shown in Figs. 2 and 5 that the inhibition rate of cell proliferation was significantly higher in the BC600 treatment than in the BC200 and BC400 treatments. Meanwhile, the top 20 DEMs were all significantly upregulated in the BC200 treatment (Fig. 6). However, among the top 20 DEMs, 13 were downregulated by BC400, and 11 were downregulated due to BC600. Organic acids and derivatives were the most important category among the DEMs, and their proportion increased from 12.95% in BC200 to 24.68% in BC400 and then to 28.57% in BC600 (Fig. 7). The proportions of organoheterocyclic compounds as well as nucleosides, nucleotides, and analogues also increased with increasing pyrolysis temperature. It was suggested that microorganisms tend to change their metabolic products in response to stressful circumstances (Feofilova, 2003). The energy metabolism pathways, *e.g*., citrate cycle (tricarboxylic acid cycle), pentose phosphate pathway, pentose and glucuronate interconversions, ascorbate and aldarate metabolism, 2-oxocarboxylic acid metabolism, and biosynthesis of amino acids, were up- or downregulated in the BC200 treatment (Fig. 8a, b). Purine and pyrimidine

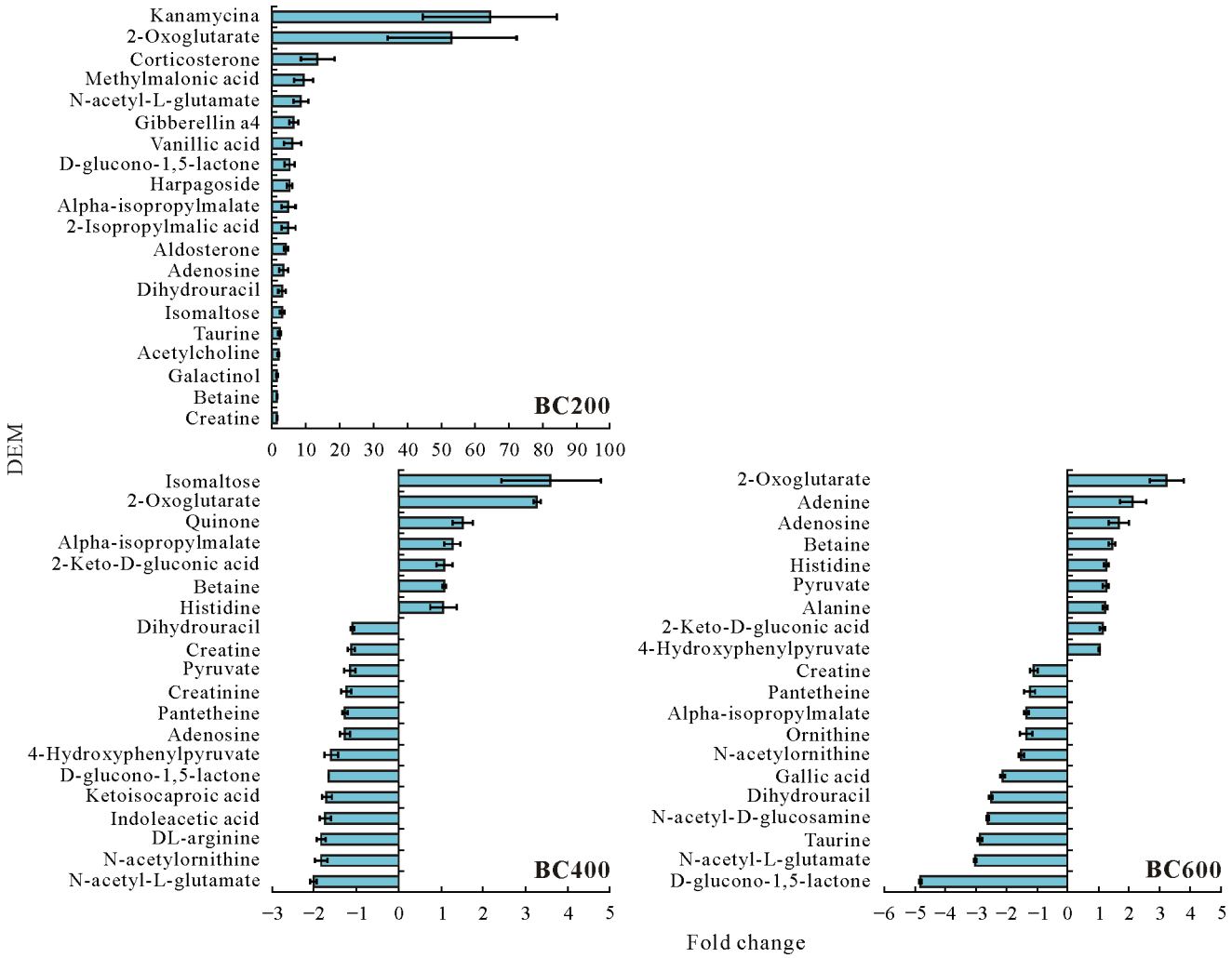

Fig. 6 Fold changes of the top 20 differentially expressed metabolites (DEMs) of the P-solubilizing bacterium *Bacillus megaterium* after 24-h incubation in Pikovskaya's medium with addition of 0.5% biochar (BC) prepared from pinewood pyrolyzed at 200 (BC200), 400 (BC400), and 600 (BC600) °C compared to no biochar addition. Error bars are standard errors of the means ($n = 3$).

metabolisms were found to be upregulated and downregulated, respectively, in the BC600 treatment (Fig. 8e, f). The synthesis and release of AKP, the major phosphatase in the present study, depends on the phosphate-sensitive histidine kinase PhoR, a regulon. As shown in *E. coli*, phosphate sensing involves a phosphorelay between PhoR and the reaction regulator PhoB (Lee *et al*., 1989). Consequently, the observed downregulation of histidine metabolism in the BC400 treatment (Fig. 8c, d) may result in decreased synthesis of histidine kinase with subsequent blockage of the phosphorelay, which normally leads to transcription of genes belonging to the phosphate regulon (Pho) (Hirani *et al*., 2001). This phosphate regulon, first discovered in *E. coli*, controls the inorganic phosphate within a cell (Wanner and Chang, 1987). Remarkably, in most bacteria, many more genes are involved in the Pho response than genes related to P assimilation (Santos-Beneit, 2015; Martín and Liras, 2021). This indicates a diverse and important role of the phosphate regulon in controlling bacterial cell growth. Disruption of Pho would thus lead to reduced growth and ecosystem services of the affected bacteria, which may be an explanation for the highest inhibition of AKP activity occurring in the BC400 treatment. Besides, exposure to BC600 significantly affected the major enrichment pathway of cysteine and methionine metabolism, with 1 upregulated and 1 downregulated (Fig. 8), which is significant with respect to both ROS production (Madeira *et al*., 2017) and metal transport and metabolism (Farkas and Sóvágó, 2016). Exposure to BC600 had additional effects beyond those of BC200 and BC400 on nucleotide metabolism which generates purine and pyrimidine for DNA replication, RNA synthesis, and cellular energy transfer (Siddiqui and Ceppi, 2020), ATP-binding cassette transporters that link ATP hydrolysis to the active transport of a variety of substrates such as ions, sugars, lipids, sterols, peptides, proteins, and drugs (Pérez Carrillo *et al*., 2022), and the cyclic guanosine monophosphate-dependent protein kinase G (cGMP-PKG) pathway involved

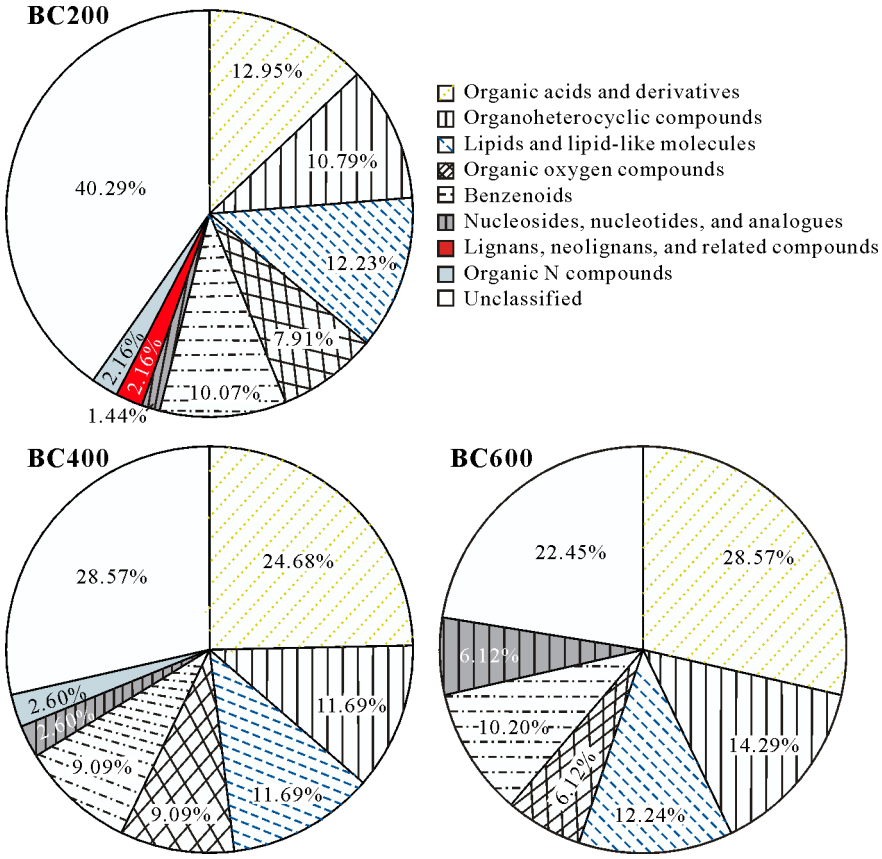

Fig. 7 Categories of the differentially expressed metabolites (DEMs) and their proportions in the total number of DEMs in the P-solubilizing bacterium *Bacillus megaterium* after 24-h incubation in Pikovskaya's medium with addition of 0.5% biochar (BC) prepared from pinewood pyrolyzed at 200 (BC200), 400 (BC400), and 600 (BC600) °C compared to no biochar addition.

in cell membrane ion channel opening, glycogenolysis, and apoptosis (Kniotek and Boguska, 2017). Furthermore, with respect to the contribution of *B. megaterium* to the P cycle, downregulation of ATP transport in the BC600 treatment likely impeded intracellular Zn transport to the master Pho regulon, whilst the modulation of the cGMP-PKG pathway likely impaired the overall cell growth (Gong *et al*., 2019) or even supported apoptosis (Kniotek and Boguska, 2017). This also meant that transmembrane transport in general could be impaired even if inorganic P and other substances to be transported were available. This supports dysfunction up to cell death and may be an explanation for the higher inhibition of cell proliferation in the BC600 treatment than in the BC200 and BC400 treatments.

CONCLUSIONS

This study investigated the cell growth or proliferation, the activity of P-related enzymes, and metabolites and related metabolic pathways of *B. megaterium* as influenced by different fractions of PW biochars produced at the temperatures of 200, 300, 400, 500, and 600 °C. The BCs and WBCs had negative effects on the cell proliferation and phosphatase activity of *B. megaterium*. Among them, BC500 and WBC500 exerted the strongest suppression on cell proliferation, while BC400 and WBC400 showed the greatest inhibition of phosphatase activity. The negative effects of high-temperature biochars on cell proliferation were mainly caused by their EPFRs, while the effects of low-temperature biochars on cell proliferation and AKP activity were highly related to their metal contents. According to the non-targeted metabolic profiling, the histidine metabolism of PSB was downregulated by BC400, and the nucleotide metabolism was interfered by BC600. The IA model confirmed our hypothesis that DBC and WBC have an antagonistic interaction in inhibiting *B. megaterium* growth, while a synergistic effect emerged regarding the inhibition of AKP activity. Thereupon, we suggest that avoiding the release of metals from low-temperature biochar and avoiding the use of high-temperature biochar may be an effective way of reducing the risks of biochar to soil P-solubilizing microorganisms and their P solubilization ability.

DECLARATION OF COMPETING INTEREST

The authors declare that they have no known competing financial interests or personal relationships that could have appeared to influence the work reported in this paper.

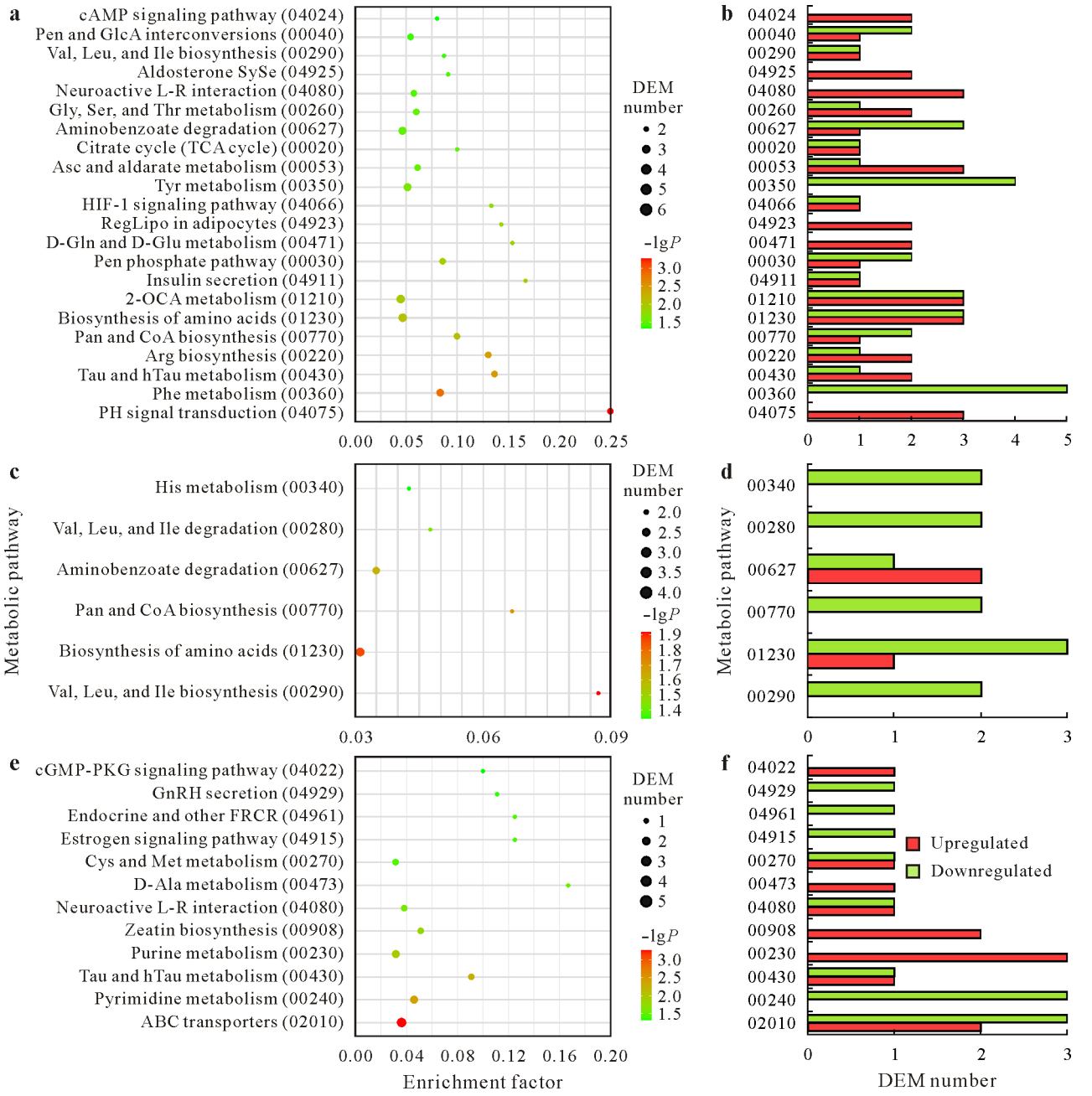

Fig. 8 Bubble diagrams of the significantly enriched metabolic pathways (a, c, and e) and numbers of differentially expressed metabolites (DEMs) in each significantly enriched metabolic pathway (b, d, and f) in the P-solubilizing bacterium *Bacillus megaterium* after 24-h incubation in Pikovskaya's medium with addition of 0.5% biochar prepared from pinewood pyrolyzed at 200 (a and b), 400 (c and d), and 600 (e and f) °C compared to no biochar addition. Pathway identifiers are in parentheses following the pathway names according to the Kyoto Encyclopedia of Genes and Genomes Pathway database. cAMP = cyclic adenosine monophosphate; Pen = pentose; GlcA = glucuronate; Val = valine; Leu = leucine; Ile = isoleucine; SySe = synthesis and secretion; L-R = ligand-receptor; Gly = glycine; Ser = serine; Thr = threonine; TCA = tricarboxylic acid; Asc = ascorbate; Tyr = tyrosine; HIF-1 = hypoxia-inducible factor-1; RegLipo = regulation of lipolysis; D-Gln = D-glutamine; D-Glu = D-glutamate; 2-OCA = 2-oxocarboxylic acid; Pan = pantothenate; CoA = coenzyme A; Arg = arginine; Tau = taurine; hTau = hypotaurine; Phe = phenylalanine; PH = plant hormone; His = histidine; cGMP-PKG = cyclic guanosine monophosphate-dependent protein kinase; GnRH = gonadotropin-releasing hormone; FRCR = factor-regulated calcium reabsorption; Cys = cysteine; Met = methionine; D-Ala = D-alanine; ABC = adenosine triphosphate-binding cassette.

ACKNOWLEDGEMENTS

This research was financially supported by the National Key Research and Development Program of China (No. 2023YFC3709104), the National Natural Science Foundation of China (No. 41967039), the Yunnan Provincial Ten Thousand Plan, China (No. YNWR-QNBJ-2019-065), the Yunnan Provincial Excellent Young Scientists Fund, China (No. 202201AW070006), and the Yunnan Major Scientific and Technological Projects, China (No. 202202AG050019).

SUPPLEMENTARY MATERIAL

Supplementary material for this article can be found in the online version.

REFERENCES

Alori E T, Glick B R, Babalola O O. 2017. Microbial phosphorus solubilization and its potential for use in sustainable agriculture. *Front Microbiol*. **8**: 971.

Ammerman J W, Azam F. 1985. Bacterial 5-nucleotidase in aquatic ecosystems: A novel mechanism of phosphorus regeneration. *Science*. **227**: 1338–1340.

An M J, Chang D D, Hong D S, Fan H, Wang K Y. 2021. Metabolic regulation in soil microbial succession and niche differentiation by the polymer amendment under cadmium stress. *J Hazard Mater*. **416**: 126094.

Anthony C. 1992. The structure of bacterial quinoprotein dehydrogenases. *Int J Biochem*. **24**: 29–39.

Anuj S A, Gajera H P, Hirpara D G, Golakiya B A. 2020. The impact of bacterial size on their survival in the presence of cationic particles of nano-silver. *J Trace Elem Med Biol*. **61**:126517.

Bradshaw R A, Cancedda F, Ericsson L H, Neumann P A, Piccoli S P, Schlesinger M J, Shriefer K, Walsh K A. 1981. Amino acid sequence of *Escherichia coli* alkaline phosphatase. *Proc Natl Acad Sci USA*. **78**: 3473–3477.

Calabrese E J, Baldwin L A. 2003. Toxicology rethinks its central belief. *Nature*. **421**: 691–692.

Chen Z M, Chen B L, Chiou C T. 2012. Fast and slow rates of naphthalene sorption to biochars produced at different temperatures. *Environ Sci Technol*. **46**: 11104–11111.

Cheng Y Y, Narayanan M, Shi X J, Chen X P, Li Z L, Ma Y. 2023. Phosphate-solubilizing bacteria: Their agroecological function and optimistic application for enhancing agro-productivity. *Sci Total Environ*. **901**: 166468.

Das S K, Ghosh G K, Avasthe R K, Sinha K. 2021. Compositional heterogeneity of different biochar: Effect of pyrolysis temperature and feedstocks. *J Environ Manage*. **278**: 111501.

Demirbas A. 2004. Effects of temperature and particle size on bio-char yield from pyrolysis of agricultural residues. *J Anal Appl Pyrol*. **72**: 243–248.

Fang G D, Gao J, Liu C, Dionysiou D D, Wang Y, Zhou D M. 2014. Key role of persistent free radicals in hydrogen peroxide activation by biochar: Implications to organic contaminant degradation. *Environ Sci Technol*. **48**: 1902–1910.

Farkas E, Sóvágó I. 2016. Metal complexes of amino acids and peptides. *In* Ryadnov M, Hudecz F (eds.) Amino Acids, Peptides and Proteins. RSC, Cambridge. pp. 100–151.

Feofilova E P, 2003. Deceleration of vital activity as a universal biochemical mechanism ensuring adaptation of microorganisms to stress factors: A review. *Appl Biochem Microbiol*. **39**: 1–18.

Gong L Y, Lei Y T T, Tan X Y, Dong Y P, Luo Z Z, Zhang D, Han S X. 2019. Propranolol selectively inhibits cervical cancer cell growth by suppressing the cGMP/PKG pathway. *Biomed Pharmacother*. **111**: 1243–1248.

Hirani T A, Suzuki I, Murata N, Hayashi H, Eaton-Rye J J. 2001. Characterization of a two-component signal transduction system involved in the induction of alkaline phosphatase under phosphate-limiting conditions in *Synechocystis* sp. PCC 6803. *Plant Mol Biol*. **45**: 133–144.

Hossain Z, Bahar M, Sarkar B, Donne S W, Sik Ok Y, Palansooriya K N, Kirkham M B, Chowdhury S, Bolan N. 2020. Biochar and its importance on nutrient dynamics in soil and plant. *Biochar*. **2**: 379–420.

Ibáñez A, Diez-Galán A, Cobos R, Calvo-Peña C, Barreiro C, Medina-Turienzo J, Sánchez-García M, Coque J J R. 2021. Using rhizosphere phosphate solubilizing bacteria to improve barley (*Hordeum vulgare*) plant productivity. *Microorganisms*. **9**: 1619.

Illmer P, Schinner F. 1992. Solubilization of inorganic phosphates by microorganisms isolated from forest soils. *Soil Biol Biochem*. **24**: 389–395.

Illmer P, Schinner F. 1995. Solubilization of inorganic calcium phosphates—Solubilization mechanisms. *Soil Biol Biochem*. **27**: 257–263.

International Biochar Initiative. 2015. Standardized product definition and product testing guidelines for biochar that is used in soil. Available online at https://biochar-international.org/wp-content/uploads/2020/06/IBI_Biochar_Standards_V2.1_Final2.pdf (verified on Nov. 14, 2025).

Jakobsen I, Leggett M E, Richardson A E. 2015. Rhizosphere microorganisms and plant phosphorus uptake. *In* Sims J T, Sharpley A N (eds.) Phosphorus: Agriculture and the Environment. American Society of Agronomy, Madison. pp. 437–494.

Kaur C, Selvakumar G, Ganeshamurthy A N. 2016. Organic acids in the rhizosphere: Their role in phosphate dissolution. *In* Singh D P, Singh H B, Prabha R (eds.) Microbial Inoculants in Sustainable Agricultural Productivity. Springer, New Delhi. pp. 165–177.

Khadem A, Raiesi F. 2017. Influence of biochar on potential enzyme activities in two calcareous soils of contrasting texture. *Geoderma*. **308**: 149–158.

Kniotek M, Boguska A. 2017. Sildenafil can affect innate and adaptive immune system in both experimental animals and patients. *J Immunol Res*. **2017**: 4541958.

Kour D, Rana K L, Kaur T, Yadav N, Yadav A N, Kumar M, Kumar V, Dhaliwal H S, Saxena A K. 2021. Biodiversity, current developments and potential biotechnological applications of phosphorus-solubilizing and -mobilizing microbes: A review. *Pedosphere*. **31**: 43–75.

Lee T Y, Makino K, Shinagawa H, Amemura M, Nakata A. 1989. Phosphate regulon in members of the family Enterobacteriaceae: Comparison of the *phoB-phoR* operons of *Escherichia coli*, *Shigella dysenteriae*, and *Klebsiella pneumoniae*. *J Bacteriol*. **171**: 6593–6599.

Lehmann J, Gaunt J, Rondon M. 2006. Bio-char sequestration in terrestrial ecosystems—A review. *Mitig Adapt Strat Glob Change*. **11**: 403–427.

Li H J, Li H, Zuo N, Liu Y, Lang D, Steinberg C, Pan B, Xing B S. 2022. Direct toxicity of environmentally persistent free radicals to nematode *Caenorhabditis elegans* after excluding the concomitant chemicals. *Sci Total Environ*. **839**: 156226.

Liang L Y, Zhao Y T, Zhang L L, Kang Y B, Miao P, Zhao S M, Li S J. 2020. Identification and phosphorus solubilizing ability of *Bacillus megaterium* from rhizospheric soils of tobacco plants. *Chin J Soil Sci* (in Chinese). **51**: 1461–1466.

Lieke T, Zhang X C, Steinberg C E W, Pan B. 2018. Overlooked risks of biochars: Persistent free radicals trigger neurotoxicity in *Caenorhabditis elegans*. *Environ Sci Technol*. **52**:7981–7987.

Ling T Y, Achberger E C, Drapcho C M, Bengtson R L. 2002. Quantifying adsorption of an indicator bacteria in a soil-water system. *Trans ASAE*. **45**: 669–674.

Liu Y, Dai Q Y, Jin X Q, Dong X D, Peng J, Wu M, Liang N, Pan B, Xing B S. 2018. Negative impacts of biochars on urease activity: High pH, heavy metals, polycyclic aromatic hydrocarbons, or free radicals? *Environ Sci Technol*. **52**: 12740–12747.

Liu Y, Li Y, Pan B, Zhang X Y, Zhang H, Steinberg C E W, Qiu H, Vijver M G, Peijnenburg W J G M. 2021. Application of low dosage of copper oxide and zinc oxide nanoparticles boosts bacterial and fungal communities in soil. *Sci Total Environ*. **757**: 143807.

Madeira J P, Alpha-Bazin B M, Armengaud J, Duport C. 2017. Methionine residues in exoproteins and their recycling by methionine sulfoxide reductase AB serve as an antioxidant strategy in *Bacillus cereus*. *Front Microbiol*. **8**: 1342.

Martín J F, Liras P. 2021. Molecular mechanisms of phosphate sensing, transport and signalling in *Streptomyces* and related actinobacteria. *Int J Mo Sci*. **22**: 1129.

Mashek D G, Coleman R A. 2006. Cellular fatty acid uptake: The contribution of metabolism. *Curr Opin Lipidol*. **17**: 274–278.

Ozturk M, Metin M, Altay V, De Filippis L, Ünal B T, Khursheed A, Gul A, Hasanuzzaman M, Nahar K, Kawano T, Caparrós P G. 2021. Molecular biology of cadmium toxicity in *Saccharomyces cerevisiae*. *Biol Trace Elem Res*. **199**: 4832–4846.

Pan B, Li H, Lang D, Xing B S. 2019. Environmentally persistent free radicals: Occurrence, formation mechanisms and implications. *Environ Pollut*. **248**: 320–331.

Park Y, Solhtalab M, Thongsomboon W, Aristilde L. 2022. Strategies of organic phosphorus recycling by soil bacteria: Acquisition, metabolism, and regulation. *Environ Microbiol Rep*. **14**: 3–24.

Pérez Carrillo V H, Rose-Sperling D, Tran M A, Wiedemann C, Hellmich U A. 2022. Backbone NMR assignment of the nucleotide binding domain of the *Bacillus subtilis* ABC multidrug transporter BmrA in the post-hydrolysis state. *Biomol NMR Assign*. **16**: 81–86.

Pikovskaya R I. 1948. Mobilization of phosphorus in soil connection with the vital activity of some microbial species. *Microbiology*. **17**: 362–370.

Quilliam R S, Glanville H C, Wade S C, Jones D L. 2013a. Life in the 'charosphere'—does biochar in agricultural soil provide a significant habitat for microorganisms? *Soil Biol. Biochem*. **65**: 287–293.

Quilliam R S, Rangecroft S, Emmett B A, Deluca T H, Jones D L. 2013b. Is biochar a source or sink for polycyclic aromatic hydrocarbon (PAH) compounds in agricultural soils? *GCB Bioenergy*. **5**: 96–103.

Rafiq M K, Bachmann R T, Rafiq M T, Shang Z H, Joseph S, Long R L. 2016. Influence of pyrolysis temperature on physico-chemical properties of corn stover (*Zea mays* L.) biochar and feasibility for carbon capture and energy balance. *PLOS ONE*. **11**: e0156894.

Santos-Beneit F. 2015. The Pho regulon: A huge regulatory network in bacteria. *Front Microbiol*. **6**: 402.

Shi R Y, Ni N, Nkoh Nkoh J, Dong Y, Zhao W R, Pan X Y, Li J Y, Xu R K, Qian W. 2020. Biochar retards Al toxicity to maize (*Zea mays* L.) during soil acidification: The effects and mechanisms. *Sci Total Environ*. **719**: 137448.

Siddiqui A, Ceppi P. 2020. A non-proliferative role of pyrimidine metabolism in cancer. *Mol Metab*. **35**: 100962.

Spokas K A, Novak J M, Stewart C E, Cantrell K B, Uchimiya M, DuSaire M G, Ro K S. 2011. Qualitative analysis of volatile organic compounds on biochar. *Chemosphere*. **85**: 869–882.

Suliman W, Harsh J B, Fortuna A M, Garcia-Pérez M, Abu-Lail N I. 2017. Quantitative effects of biochar oxidation and pyrolysis temperature on the transport of pathogenic and nonpathogenic *Escherichia coli* in biochar-amended sand columns. *Environ Sci Technol*. **51**: 5071–5081.

Sun L, Gong M Y, Lv X Q, Huang Z Y, Gu Y, Li J H, Du G C, Liu L. 2020. Current advance in biological production of short-chain organic acid. *Appl Microbiol Biot*. **104**: 9109–9124.

Uchimiya M, Wartelle L H, Klasson K T, Fortier C A, Lima I M. 2011. Influence of pyrolysis temperature on biochar property and function as a heavy metal sorbent in soil. *J Agric Food Chem*. **59**: 2501–2510.

Wang L P, Xia Q, Li Y F. 2017. The effects of high pressure processing and slightly acidic electrolysed water on the structure of *Bacillus cereus* spores. *Food Control*. **79**: 94–100.

Wanner B L, Chang B D. 1987. The phoBR operon in *Escherichia coli* K-12. *J Bacteriol*. **169**: 5569–5574.

Warnock D D, Mummey D L, McBride B, Major J, Lehmann J, Rillig M C. 2010. Influences of non-herbaceous biochar on arbuscular mycorrhizal fungal abundances in roots and soils: Results from growth-chamber and field experiments. *Appl Soil Ecol*. **46**: 450–456.

Wongrod S, Simon S, Guibaud G, Lens P N L, Pechaud Y, Huguenot D, van Hullebusch E D. 2018. Lead sorption by biochar produced from digestates: Consequences of chemical modification and washing. *J Environ Manage*. **219**: 277–284.

Yakout S M. 2017. Physicochemical characteristics of biochar produced from rice straw at different pyrolysis temperature for soil amendment and removal of organics. *Proc Natl Acad Sci India Sect A Phys Sci*. **87**: 207–214.

Yan T T, Ding Z J, Zhu Q, Bu X L, Xue J H, Wu Y B. 2018. Effects of biochar on physicochemical properties of yellow-brown soil and growth of *Cinnamomum camphora* seedlings. *Soils* (in Chinese). **50**: 681–686.

Yang X H, Zhong Y P, Wang D, Lu Z T. 2021. A simple colorimetric method for viable bacteria detection based on cell counting Kit-8. *Anal Methods*. **13**: 5211–5215.

Yu L Y, Huang H B, Wang X H, Li S, Feng N X, Zhao H M, Huang X P, Li Y W, Li H, Cai Q Y, Mo C H. 2019. Novel phosphate-solubilising bacteria isolated from sewage sludge and the mechanism of phosphate solubilisation. *Sci Total Environ*. **658**: 474–484.

Yuan S, Zhao L X, Meng H B, Shen Y J. 2016. The main types of biochar and their properties and expectative researches. *J Plant Nutr Fertrl* (in Chinese). **22**: 1402–1417.

Zhang K, Mao J F, Chen B L. 2019. Reconsideration of heterostructures of biochars: Morphology, particle size, elemental composition, reactivity and toxicity. *Environ Pollut*. **254**: 113017.

Zhang Y, Han M, Si X H, Bai L L, Zhang C X, Quan X. 2022. Toxicity of biochar influenced by aging time and environmental factors. *Chemosphere*. **298**: 134262.

Zhu H X, Liu X Y, Jiang Y, Zhang M, Lin D H, Yang K. 2021. Time-dependent desorption of anilines, phenols, and nitrobenzenes from biochar produced at 700 °C: Insight into desorption hysteresis. *Chem Eng J*. **422**: 130584.

Zhu Y L, Liu C L, You Y, Liu J, Guo Y H, Han J G. 2019. Magnitude of the mixture hormetic response of soil alkaline phosphatase can be predicted based on single conditions of Cd and Pb. *Ecotoxicology*. **28**: 790–800.